AGU ADVANCING EARTH AND SPACE SCIENCE

Geophysical Research Letters

RESEARCH LETTER
10.1029/2022GL101073

Multidecadal Intensification of Atlantic Tropical Instability Waves

Franz Philip Tuchen[1], Renellys C. Perez[1], Gregory R. Foltz[1], Peter Brandt[2,3], and Rick Lumpkin[1]

[1]NOAA/Atlantic Oceanographic and Meteorological Laboratory, Miami, FL, USA, [2]GEOMAR Helmholtz Centre for Ocean Research Kiel, Kiel, Germany, [3]Faculty of Mathematics and Natural Sciences, Kiel University, Kiel, Germany

Key Points:

- In situ and satellite observations show a long-term intensification of Tropical Instability Waves (TIWs) in the tropical North Atlantic
- Enhanced TIW activity is mainly due to increased barotropic instability associated with increased covariance of velocity fluctuations
- As a result, TIW-driven sea surface cooling north of the equator due to eddy temperature advection has increased by 74% from 1993 to 2021

Supporting Information:

Supporting Information may be found in the online version of this article.

Correspondence to:

F. P. Tuchen,
franz.philip.tuchen@noaa.gov;
fptuchen@gmx.de

Citation:

Tuchen, F. P., Perez, R. C., Foltz, G. R., Brandt, P., & Lumpkin, R. (2022). Multidecadal intensification of Atlantic tropical instability Waves. *Geophysical Research Letters*, *49*, e2022GL101073. https://doi.org/10.1029/2022GL101073

Received 1 SEP 2022
Accepted 4 NOV 2022

Abstract

Tropical Instability Waves (TIWs) are the dominant source of intraseasonal variability in the central equatorial Atlantic and play an important role in the redistribution of heat in the upper ocean. Here we use multidecadal records of sea surface temperature, sea level anomaly, sea surface salinity, and near-surface currents constructed from in situ and satellite observations to reveal a long-term intensification of the intraseasonal variability of these variables due to an increase of TIW activity. Enhanced barotropic energy conversion from increased covariance of horizontal current fluctuations, rather than low-frequency changes of the mean zonal currents, drives the TIW intensification. As a consequence, boreal summer cooling of tropical North Atlantic surface waters through horizontal eddy temperature advection increased by 0.03°C month^{-1} decade^{-1} during 1993–2021, a change of 74% ± 53% relative to the long-term mean. The presented multidecadal TIW trends are strongly modulated by interannual variations like the 2021 Atlantic Niño.

Plain Language Summary

In the equatorial Atlantic, temperature, salinity, sea level anomaly, and ocean velocity variations on time scales of tens of days are dominated by the presence and westward passage of large-scale Tropical Instability Waves (TIWs). Several decades of satellite and surface drifter data as well as moored velocity observations show a long-term intensification of TIW activity in all of these variables in the tropical North Atlantic where TIWs are most pronounced. We find that increased high-frequency flow variability, and not long-term changes of the mean zonal current system, drives the TIW intensification. One consequence of increased Atlantic Ocean TIW activity is the corresponding intensification of the horizontal eddy temperature advection pattern in boreal summer leading to stronger cooling of surface waters north of the equator. This equates to an increase in TIW-driven sea surface temperature cooling of 74% ± 53% in the tropical North Atlantic during the last 3 decades. The presented multidecadal TIW trends are strongly modulated by interannual variations such as the 2021 Atlantic Niño. We further explore potential large-scale drivers of the TIW intensification, including changes in high-frequency wind variability.

1. Introduction

The upper-ocean circulation in the tropical Atlantic is characterized by energetic zonal currents that facilitate a large cross-basin volume exchange and transformation of water masses (e.g., Brandt et al., 2006; Lumpkin & Garzoli, 2005; Tuchen, Brandt, Lübbecke, & Hummels, 2022). Near the equator, the lateral and vertical shear of the zonal currents generates barotropic and baroclinic instability that supply eddy kinetic energy for the formation of Tropical Instability Waves (TIWs) (de Decco et al., 2018; Jochum et al., 2004; Masina et al., 1999; von Schuckmann et al.; 2008; Weisberg & Weingartner, 1988). TIWs are observable as quasi-monthly, westward-propagating anomalies of key ocean variables such as sea surface temperature (SST), sea surface salinity (SSS), sea level, and currents (Athié & Marin, 2008; Bunge et al., 2007; Foltz et al., 2004; Grodsky et al.; 2005; Olivier et al., 2020; Perez et al., 2019; Tuchen et al., 2018).

TIWs redistribute heat and freshwater through advection and mixing (Foltz et al., 2020; Hummels et al., 2013; Inoue et al., 2019; Jochum & Murtugudde, 2006; Jochum et al., 2007; Kennan & Flament, 2000; Moum et al., 2009; Wenegrat & McPhaden, 2015) and affect the biogeochemistry of the equatorial upper ocean by influencing chlorophyll concentration (Grodsky et al., 2008; Menkes et al., 2002; Sherman et al., 2022; Shi & Wang, 2021), dissolved oxygen variability (Eddebbar et al., 2021), and nitrate distributions (Radenac et al., 2020). Through their impact on SST, TIWs also feed back onto the large-scale atmospheric circulation (Caltabiano et al., 2005;

Seo & Xie, 2011; Seo et al., 2007; Wu & Bowman, 2007b). More recently, TIWs and intraseasonal waves excited by TIWs have been identified as an important component and maintenance mechanism of the deep equatorial Atlantic circulation (Ascani et al., 2010, 2015; Bastin et al., 2020; Greatbatch et al., 2018; Körner et al., 2022; Tuchen et al., 2018).

Although the seasonality of Atlantic TIW activity is well documented (Grodsky et al., 2005; Heukamp et al., 2022; Olivier et al., 2020; Perez et al., 2012; Specht et al., 2021; Tuchen et al., 2018), considerably less is known about interannual to decadal variability and long-term trends of TIWs and the associated variability of physical and biogeochemical properties. Previous studies identified significant year-to-year variability of TIWs (Athié & Marin, 2008; Caltabiano et al., 2005; Olivier et al., 2020; Perez et al., 2012; Wu & Bowman, 2007a) and suggested the coupled Atlantic zonal mode and changes in the barotropic energy conversion as possible sources for the observed interannual fluctuations (Perez et al., 2012; Wu & Bowman, 2007a). Jochum and Murtugudde (2004) showed that internal variability can be an important driver of interannual TIW variability. Beyond interannual time scales, even less is known about TIW variability and trends on decadal to multidecadal time scales. Recent studies suggest that upper-ocean currents at low latitudes in the Pacific and Atlantic have experienced a global warming-induced intensification that is discernible in enhanced mean kinetic energy (Hu et al., 2020; Peng et al., 2022; Wunsch, 2020). Moored velocity observations in the central equatorial Atlantic seem to support these findings by showing a substantial increase of the Equatorial Undercurrent (EUC) and the westward surface current above the EUC between 2008 and 2018 (Brandt et al., 2021). However, this recent intensification of the Atlantic EUC has been attributed mainly to decadal-multidecadal variability of the wind-driven shallow overturning circulation (Tuchen et al., 2020) rather than being a response to global warming. One expected consequence of a spin-up of the equatorial zonal current system is an increase in meridional and vertical shear of the zonal currents, potentially leading to intensified barotropic and baroclinic energy conversion, respectively, from the mean flow to high-frequency velocity (i.e., eddy) variability. Decadal changes in Atlantic TIW activity, and possible connections to the global ocean circulation spin-up, have not yet been examined. This study identifies long-term trends of Atlantic TIW activity in SST, sea level anomaly (SLA), velocity, and SSS, investigates their potential causes, and highlights the effect of the observed long-term TIW intensification on TIW-induced horizontal eddy temperature advection (ETA) in the tropical North Atlantic.

2. Data and Methods

Multidecadal gridded (satellite, reanalysis winds, blended satellite-in situ) and mooring records are used in this study. All gridded data are available at daily and 0.25° horizontal resolution. SST from the NOAA Optimally Interpolated SST data set (OI-SST version 2.1) is available since September 1981 (Huang et al., 2021). SLA data are provided by the Copernicus Marine Environment Monitoring Service since January 1993 (version vDT2021). To obtain homogeneous data coverage, a two-satellite constellation is used in vDT2021. SSS data are provided by the European Space Agency Sea Surface Salinity Climate Change Initiative (ESA-SSS-CCI version 3.21) between January 2010 and September 2020 (Boutin et al., 2021). For the purpose of this study only full-year data of SST (1982–2021) and SLA (1993–2021) are used. Because of the more limited observational period of SSS, the available record between 2010 and 2020 is included in the analysis, but we focus mainly on SST and SLA. It is important to note that only the surface signatures of TIWs can be inferred from satellite observations. The surface patterns differ from those in the subsurface (Perez et al., 2019; Specht et al., 2021; Wenegrat & McPhaden, 2015), likely due to the baroclinicity of the mean zonal flow: the surface mean flow is dominated by the North Equatorial Counter Current (NECC) and the northern and central branches of the South Equatorial Current (nSEC/cSEC), while the equatorial thermocline is dominated by the EUC.

Estimates of the near-surface circulation at an approximate depth of 15 m are available from a synthesis product of surface drifting buoy velocities, satellite-derived Ekman velocities, and geostrophic velocities from the SLA product described above (Lumpkin & Garzoli, 2011). The most recent version of the drifter-wind-altimetry synthesis covers the time period from 1993 to 2021 and provides daily horizontal current velocities at 0.25° horizontal resolution (Perez et al., 2019). A more detailed description, validation and uncertainty assessment of this synthesis is provided in the Supporting Information S1.

Moored velocity data have been collected at 0°, 23°W since 2001 and at 4°N, 23°W since 2005 as part of the tropical Atlantic observing system (Foltz et al., 2019) and the Prediction and Research Moored Array in the Tropical Atlantic (PIRATA; Bourlès et al., 2019). Moored velocity observations provide an important subsurface view of

TIW variability and trends. A detailed description of the individual measurements and their combination into one uniform data set at 0°, 23°W is provided by Tuchen, Brandt, Hahn, et al. (2022). Here we mainly investigate continuous subsurface (20–100 m) velocities available between March 2008 and October 2019. We focus on the meridional component of velocity (v) because there tend to be larger meridional velocity fluctuations at and north of the equator than zonal velocity (u) fluctuations (Perez et al., 2019; Tuchen et al., 2018).

To identify and quantify TIW activity, first all data are temporally band-pass filtered (20–50 day Hamming window). In a second step, those data sets that exhibit spatial dimensions are zonally band-pass filtered (4°–20°) following established Atlantic TIW methodology (Lee et al., 2014; Olivier et al., 2020; Perez et al., 2012). Then, for a filtered time series x', the monthly standard deviation $\sigma(x')$ is calculated and the resulting monthly standard deviation time series will be used as a proxy for TIW activity/variability in the subsequent statistical analysis. In the following, long-term averages are denoted by an overbar and seasonal averages are denoted by subscripts indicating the incorporated months. For instance, $\overline{\sigma\left(\mathrm{SST}'\right)_{\mathrm{JJA}}}$ describes the mean intraseasonal (temporally and spatially band-pass filtered) standard deviation of SST, created by averaging the monthly standard deviations from June, July, and August either at a grid point or spatially averaged within a specific region. Throughout this study, error estimates are based on a linear regression analysis with 95% confidence intervals (Brandt et al., 2021), assuming each monthly standard deviation represents one degree of freedom.

3. Results

3.1. Spatio-Temporal Mean of TIW Activity

First, we identify the long-term mean spatial and temporal distributions of intraseasonal variability associated with TIWs, which we will then use in the next section to determine temporal changes of the mean variability patterns over the individual observational periods. In agreement with previous studies (Athié & Marin, 2008; Perez et al., 2012), $\sigma(\mathrm{SST}')$ shows maximum values at 0°–5°N between 30°–10°W (Figure 1a), while $\sigma(\mathrm{SLA}')$ peaks further north between 3°N–7°N (Figure 1c). $\sigma(\mathrm{SLA}')$ is co-located with $\sigma(v')$ as obtained from the drifter-wind-altimetry synthesis (Figures 1c and 1e), in which, however, equatorial v' is underrepresented (Figure S1 in Supporting Information S1). TIW-associated variability is spatially separable from other processes with similar time scales, such as high $\sigma(\mathrm{SLA}')$ and $\sigma(v')$ within the North Brazil Current retroflection area. Modest TIW-induced variability is also observed south of the equator, in agreement with previous findings (Athié & Marin, 2008; Perez et al., 2012; Yu et al., 1995). Here we focus on changes in the region of highest variability north of the equator. Within this region, the seasonal cycle and the months with highest intraseasonal variability are identified: $\sigma(\mathrm{SST}')$ peaks in July (Figure 1b), while $\sigma(v')$ and $\sigma(\mathrm{SLA}')$ show matching spatial and temporal patterns north of the equator, with a maximum in July and second largest value in June (Figures 1d and 1f). This indicates that $\sigma(v')$ and $\sigma(\mathrm{SLA}')$ precede $\sigma(\mathrm{SST}')$. Although the satellite SSS record is considerably shorter, there is also a clear signature of TIWs with peak $\sigma(\mathrm{SSS}')$ variability north of the equator that is strongest in June (Figures S2a and S2b in Supporting Information S1), consistent with previous findings (Lee et al., 2014; Olivier et al., 2020).

To obtain a subsurface view of TIW activity, we examine the 0°, 23°W moored velocity observations. The 20–50 m average of mean intraseasonal meridional velocity variability shows an annual peak during July–September (Figures S3a and S3b in Supporting Information S1) that lags the June/July peak in near-surface meridional velocity variability north of the equator (Figure 1f). The NECC/nSEC and nSEC/EUC regions are two separate generation sites for TIWs (von Schuckmann et al., 2008), which partly explains the difference in these timings.

3.2. Long-Term Trends of TIW Activity

Long-term trends of monthly standard deviations of SST′, SLA′, and v' are calculated at each grid point for their respective time periods and reported in terms of unit change per decade (Figure 2). Increasing variability is observed for all variables over the observational period in the previously identified regions of highest mean variability (Figures 2a, 2d and 2g). The spatial patterns of the trends largely align with the climatological patterns (Figures 1a, 1c and 1e) and reveal long-term intensification of intraseasonal variability. The TIW intensification generally occurs during the climatological peak months, especially for $\sigma(\mathrm{SST}')$ and $\sigma(\mathrm{SSS}')$ (Figure 2b; Figure S2d in Supporting Information S1). Interestingly, $\sigma(\mathrm{SSS}')$ exhibits a strong positive trend between 2010 and

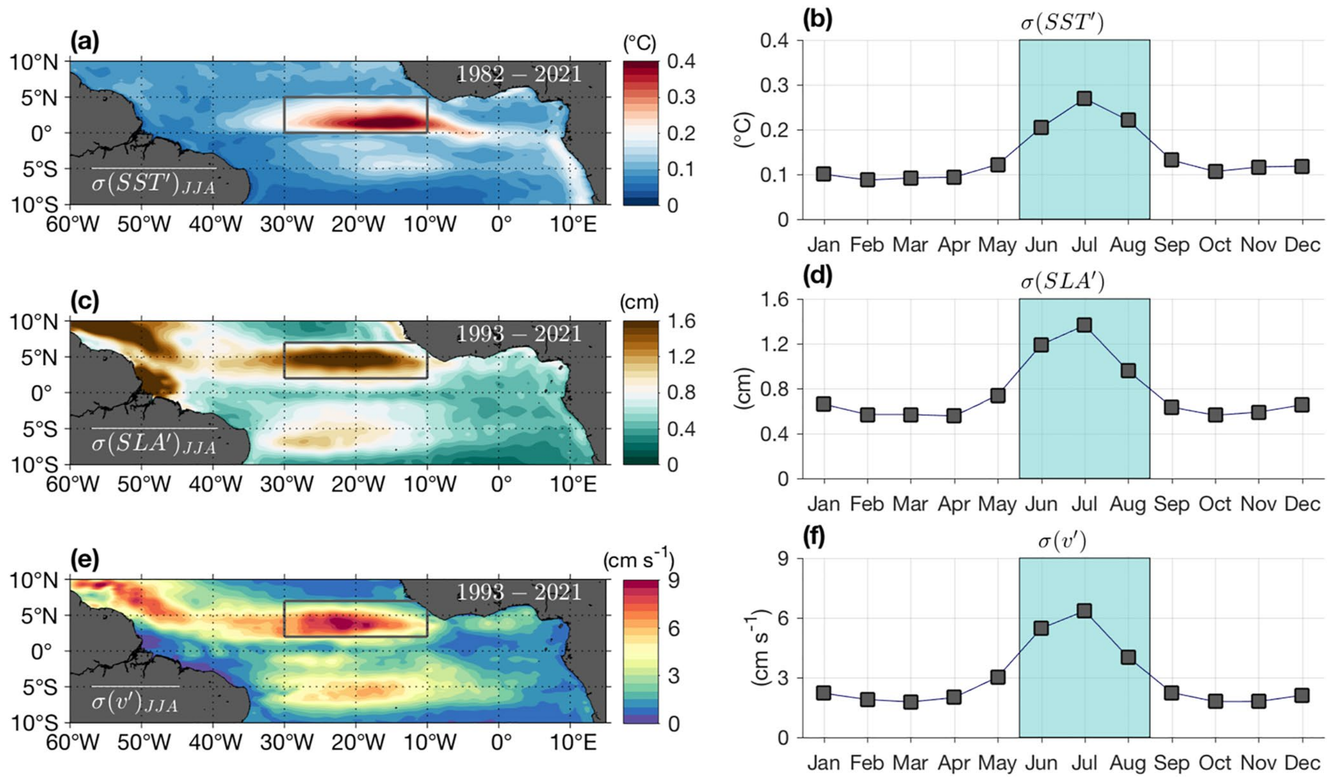

Figure 1. Long-term mean of intraseasonal variability for oceanic sea surface variables associated with Tropical Instability Waves (TIWs). Standard deviation (σ) of band-pass filtered (a, b) sea surface temperature (SST′), (c, d) sea level anomaly (SLA′), (e, f) meridional velocity (v'). Left panels: Mean of the monthly σ averaged over June to August (JJA) during peak TIW season indicated by the turquoise shaded box in the right panels. Right panels: Spatial averages of monthly σ in the boxes and for the multidecadal time period indicated in the left panels.

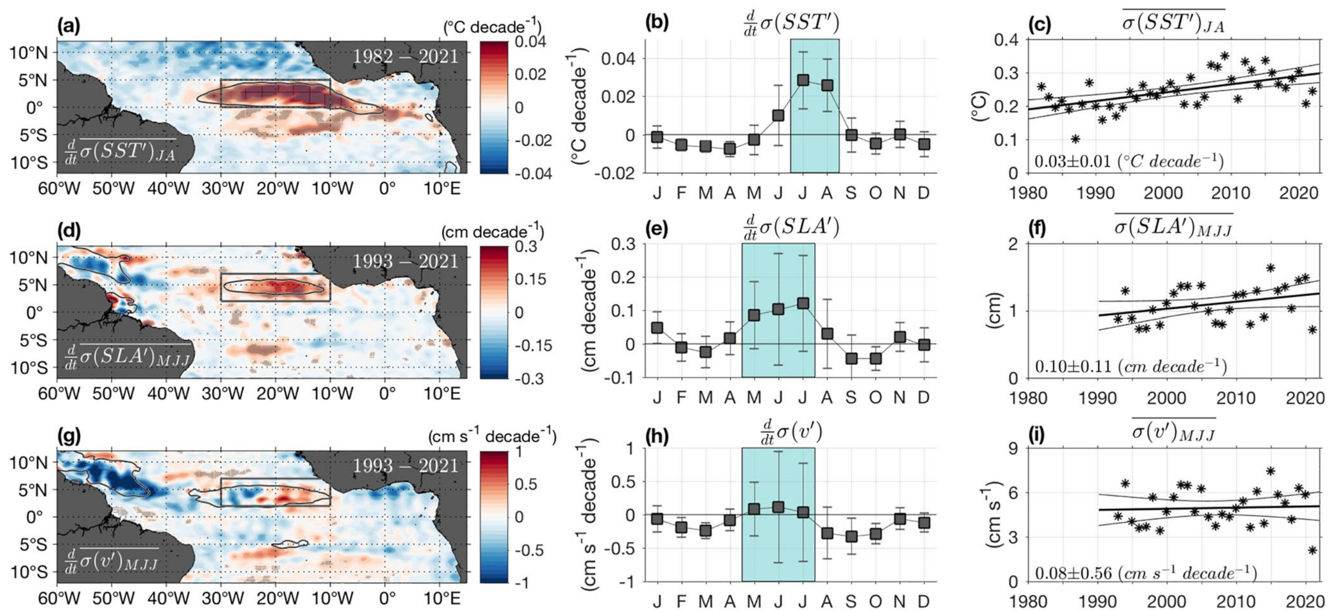

Figure 2. Long-term linear trends of the standard deviation of band-pass filtered (a–c) sea surface temperature (SST′), (d–f) sea level anomaly (SLA′), and (g–i) meridional velocity (v') in units per decade. In the left panels, significant trends are indicated by gray dots and one background Tropical Instability Wave (TIW) variability isoline from Figure 1 is shown (black lines: 0.2°C, 1.5 cm, 5 cm s^{-1}). Monthly TIW activity trends in the middle panels are spatially averaged over the boxes indicated in the left panels. The time series in the right panels show the yearly composite values averaged over the boxes in the left panels and the months shaded in turquoise in the middle panels. Solid thin lines indicate the 95% confidence band.

2020 during all months (Figures S2d and S2e in Supporting Information S1), but the relatively short observational record of $\sigma(\mathrm{SSS}')$ is likely obscured by interannual to decadal variability. $\sigma(\mathrm{SLA}')$ shows a tendency for a temporal shift toward a 1-month earlier onset of TIW activity (Figure 2e) that is also observed in moored velocity observations on the equator (Figure S3c in Supporting Information S1). The overall trends reveal intensification of TIW activity with respect to the long-term mean: $\sigma(\mathrm{SST}')$ intensified by 43% ± 19% during 1982–2021 (Figures 2a–2c), $\sigma(\mathrm{SLA}')$ increased by 26% ± 30% during 1993–2021 (Figures 2d–2f), while $\sigma(v')$ shows only a weak intensification of 4% ± 33% during 1993–2021 east of 20°W (Figures 2g–2i). The trends are larger when the strong Atlantic Niño year of 2021 is excluded: 48% ± 18%, 35% ± 28%, and 17% ± 29% for $\sigma(\mathrm{SST}')$, $\sigma(\mathrm{SLA}')$, and $\sigma(v')$ respectively.

Below the surface, $\sigma(v')$ at 0°, 23°W increased from 2008 to 2018 during May, June and especially July (Figure S3c in Supporting Information S1). Thus, there is a shift of the July–September subsurface TIW peak toward an earlier onset of the TIW season that is consistent with the near-surface temporal shift north of the equator from the drifter-wind-altimetry synthesis analysis (Figure 2h). Considering that the agreement between near-surface velocities from the drifter-wind-altimetry synthesis and moored velocities is best at 4°N, 23°W (Figure S1 in Supporting Information S1), where $\sigma(\mathrm{SST}')$ amplitudes are larger, we have more confidence in the $\sigma(v')$ trends between 3°N and 7°N and focus the remainder of our analysis on that region.

3.3. Changes in Barotropic Energy Conversion

Next, the mechanism driving the observed intensification of TIW activity north of the equator is investigated. As previously mentioned, TIWs are generated by barotropic and/or baroclinic instability. From observations presented in this study, only the barotropic energy conversion can be derived because the baroclinic energy conversion term requires knowledge of vertical velocity and density variability at temporal and spatial resolutions that are not available from observational records. Model simulations showed that barotropic energy conversion exceeds baroclinic energy conversion near the surface and between 30°W and 10°W, and thus we are analyzing a key source of TIW energy in the region (Jochum et al., 2004; von Schuckmann et al., 2008). The barotropic energy conversion term can be expressed as $\overline{BT} = -\rho_0 \cdot \overline{u'v'} \cdot d\overline{U}/dy$ (Masina et al., 1999), with a reference density $\rho_0 = 1024\ \mathrm{kg\ m^{-3}}$, primes indicating 20–50 day band-pass filtered velocities, and $\overline{U}$ the zonal background flow (50 day low-pass filtered zonal velocity). Here we use velocities from the drifter-wind-altimetry synthesis to reconstruct the near-surface barotropic energy conversion (Figure 3).

Maximum $\overline{BT}$ is observed in June/July in the region of high meridional shear of zonal velocity between the westward nSEC and the eastward NECC, approximately 2°–5°N (Figure 3a). In contrast to von Schuckmann et al. (2008), the drifter-wind-altimetry synthesis does not resolve another band of enhanced barotropic energy conversion close to the equator, though its existence is implied by moored velocity observations of $u'v'$ (Figure S4 in Supporting Information S1). $\overline{BT}$ intensified by 65% ± 92% during 1993–2021 in the tropical North Atlantic (Figures 3b–3d) during May-June. An intensification of the eddy term $\overline{u'v'}$ in May-June has driven the overall increase in barotropic energy conversion (red squares in Figure 3c), while changes of $d\overline{U}/dy$ are marginal (blue curve in Figure 3c). This is unexpected in light of recent findings on the long-term acceleration of tropical zonal currents.

One possible mechanism for increased high-frequency current fluctuations is enhanced energy input by high-frequency wind stress variability. Meridional wind stress variability at TIW time scales shows a large-scale intensification over the tropical Atlantic during the last four decades that is significant from May to September (Figure S5 in Supporting Information S1). Although the intensification of wind stress variability appears more widespread than the distinct spatio-temporal pattern of TIW variability, increased wind stress variability could fuel stronger TIW activity through the eddy term in regions and months during which TIWs develop regularly. However, this proposed mechanism deserves further attention.

3.4. Changes in Horizontal Eddy Temperature Advection

We next investigate the impact of intensified TIW activity in the equatorial Atlantic on TIW-induced horizontal ETA: $-(u'dT'/dx + v'dT'/dy)$, which is a key contributor to the SST budget in the region (Peter et al., 2006).

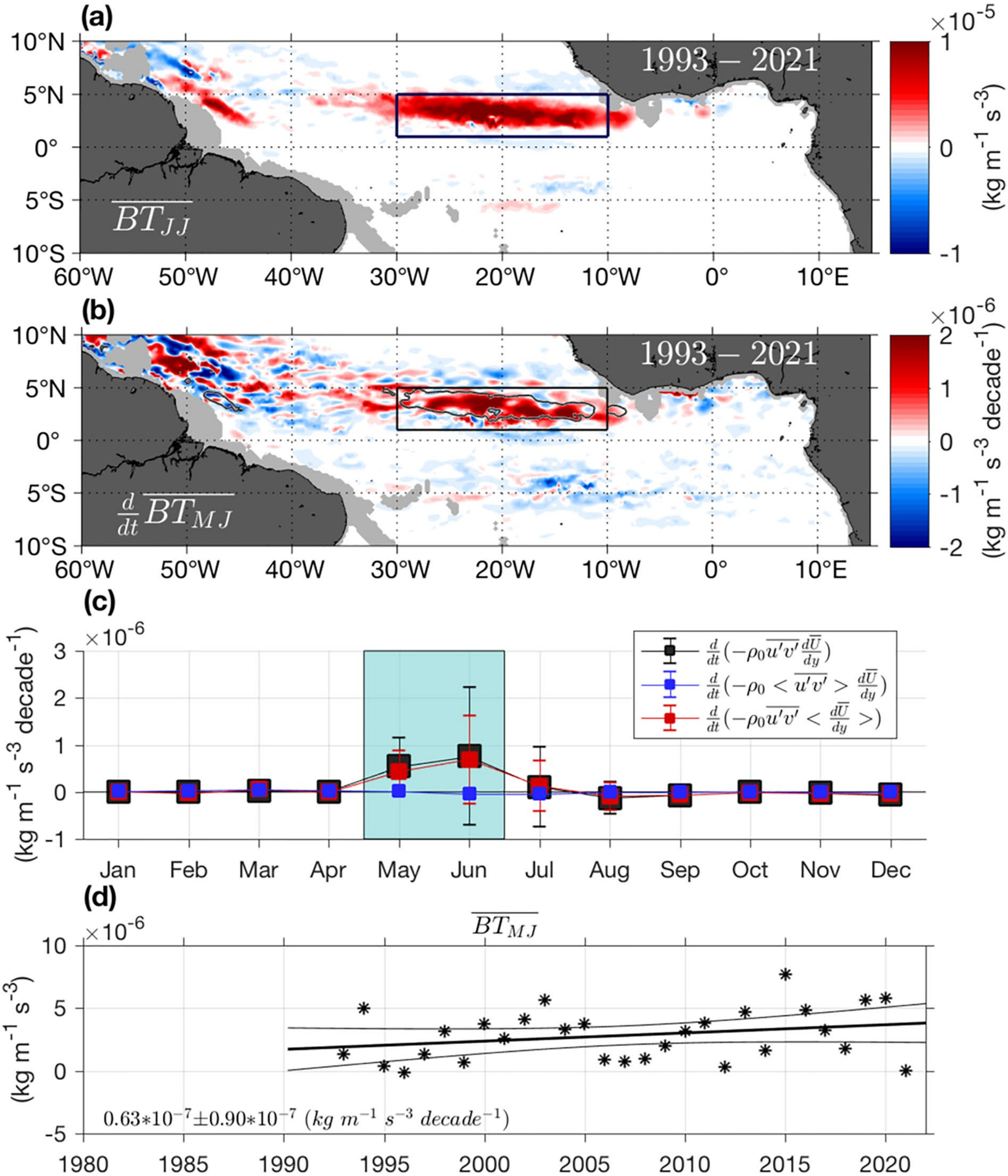

Figure 3. Near-surface (15 m) barotropic energy conversion ($\overline{BT} = -\rho_0 \cdot \overline{u'v'} \cdot d\overline{U} / dy$) in the tropical Atlantic. (a) Mean $\overline{BT}$ between 1993 and 2021 during the seasonal maximum in June/July. Positive values indicate conversion of mean kinetic energy into eddy kinetic energy, that is, intraseasonal fluctuations. (b) Trend of $\overline{BT}$ during May/June and 5×10^{-6} kg m^{-1} s^{-3} isoline from (a) (black line). (c) Monthly trends of $\overline{BT}$ (black), $\overline{BT}$ with constant $\overline{u'v'}$ (blue), and $\overline{BT}$ with constant $d\overline{U}/dy$ (red) spatially averaged over the box indicated in (a). (d) Time series of $\overline{BT}$ during May/June spatially averaged over the box indicated in (a). Solid thin lines indicate the 95% confidence band.

Here we combine near-surface velocities and satellite SST data, which is reasonable as we find good agreement between near-surface and surface velocities north of the equator (Table S1 in Supporting Information S1).

In the mean, TIWs reduce the meridional SST gradient near the equator during boreal summer, when the cold tongue reaches its maximum zonal extent (Jochum et al., 2007). TIWs advect colder equatorial surface waters northward and warmer off-equatorial surface waters equatorward (Foltz et al., 2003; Hummels et al., 2014), acting to cool the tropical North Atlantic and warm the equatorial cold tongue region. This redistribution of heat is most pronounced during June/July, with average cooling/warming rates of about 0.15°C month^{-1} (Figure 4a). Positive zonal ETA, meaning warming, occurs in the boundary region between positive and negative meridional ETA (Figure S6a in Supporting Information S1). Zonal ETA therefore supports sea surface warming close to the equator while partially but not entirely compensating sea surface cooling north of the equator caused by meridional ETA. From 1993 to 2021, this mean pattern of horizontal ETA significantly intensified (Figure 4b and 4c; Figures S6c–S6h in Supporting Information S1), leading to enhanced cooling of surface waters north of the equator of 0.03°C month^{-1} decade^{-1} and enhanced warming close to the equator of 0.02°C month^{-1} decade^{-1}. From 1993 to 2021, a 74% ± 53% increase of advective cooling north of the equator and an 85% ± 70% increase of advective warming within the cold tongue region with respect to the long-term means is observed (Figure 4d). These trends are consistent with the observed long-term intensification of TIW activity over the same period (Figures 2a–2c). Separating the ETA trends into contributions from intraseasonal velocity fluctuations and horizontal temperature gradients shows that the overall trend in ETA is driven by changes in velocities, while the temperature gradients have not changed significantly (not shown). ETA mean estimates using moored near-surface velocities at 4°N, 23°W and 0°, 23°W confirm the cooling/warming signature, but suggest an underestimation of the mean ETA pattern by the drifter-wind-altimetry product by a factor of two at 4°N and a factor of four on the equator (Figure 4a).

4. Summary and Discussion

In this study, a multidecadal intensification of TIW activity in the tropical North Atlantic is identified using essential sea surface variables. All analyzed variables (SST, SLA, SSS, surface and subsurface current velocities) agree on a long-term trend toward more intense TIW activity during boreal summer, along with a less pronounced temporal shift to an earlier onset of the TIW peak season by 1 month. For all variables, the multidecadal trends were weakened by the inclusion of data in 2021, which was an anomalously strong Atlantic Niño year characterized by weak summertime TIWs (Figure 2). The intensification of TIW activity is attributed to an increase in barotropic energy conversion that is linked to increased covariance of intraseasonal zonal and meridional velocity fluctuations and not to an enhanced meridional gradient of the zonal background flow (Figure 3). The recently reported acceleration of the tropical zonal current system seems not to have impacted zonal current shear. However, it is possible that currents that are close to being unstable supply high-frequency velocity fluctuations when being accelerated, resulting in very little change in the meridional shear of zonal velocity. In addition, here only the near-surface signature of TIW-driven variability is assessed, while the temporal evolution of the observed barotropic energy conversion as a function of depth remains a challenge and needs to be investigated in ocean models. The observational records do not allow for the estimation of baroclinic energy conversion. There are indications that baroclinic energy conversion is considerably weaker than barotropic energy conversion in the near-surface layer on seasonal time scales (Jochum et al., 2004; von Schuckmann et al., 2008), but it is not clear whether this mechanism plays a more important role on decadal time scales. The increased TIW activity reported here from satellite records is only representative of the TIWs' surface signature and is confined to the region north of the equator. Moored velocity observations have shown that TIW energy extends to depths of about 70–90 m (Heukamp et al., 2022).

A comparison of moored velocities to those from the drifter-wind-altimetry synthesis (Supporting Information S1) shows that the synthesis is suitable to analyze TIW-induced variability and trends north of the equator, where we also observe the strongest signals in the mean and trends of $\sigma(\mathrm{SST}')$ and $\sigma(\mathrm{SSS}')$ (Figure 1; Figure S2 in Supporting Information S1). Velocities from near-surface data and moored observations are weakly but positively correlated on the equator (Table S1 in Supporting Information S1). Meridional velocity trends from the drifter-wind-altimetry synthesis near the equator are weak and less pronounced compared to 4°N. However, at 0°, 23°W, we note a positive trend in $\sigma(v')$ in moored observations during 2008–2018 (Figure S3c in Supporting

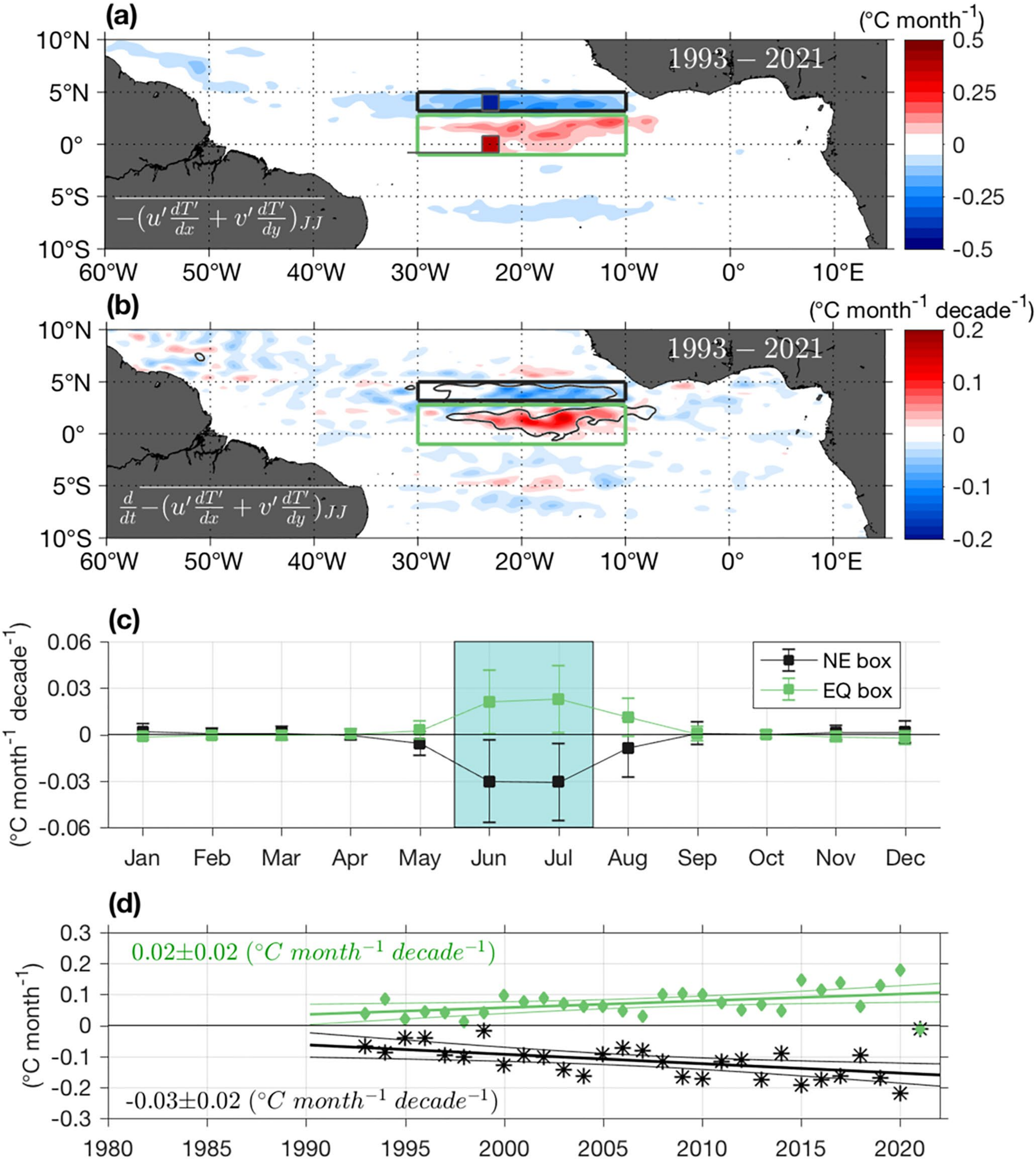

Figure 4. Near-surface (15 m) horizontal eddy temperature advection (ETA): $-(u'dT'/dx + v'dT'/dy)$ in the tropical Atlantic due to Tropical Instability Waves. (a) Mean horizontal ETA between 1993 and 2021 averaged for June/July. Positive values indicate warming, negative values indicate cooling. Also shown in (a) is the mean horizontal ETA using 10 m velocities from moored observations at 4°N, 23°W and 0°, 23°W. (b) Trend of horizontal ETA for June/July and ±0.1°C month^{-1} isoline from (a) (black lines). (c) Monthly trends of horizontal ETA in the north equatorial (NE) box and the equatorial (EQ) box indicated in (a). (d) Time series of horizontal ETA during June/July spatially averaged over the NE (black) and EQ box (green). Solid thin lines indicate the 95% confidence band.

Information S1). This underpins the necessity of sustained in situ measurements and satellite missions focusing on surface currents (Ardhuin et al., 2019; Rodríguez et al., 2019).

The observed enhanced barotropic energy conversion north of the equator is hypothesized to be related to increased high-frequency wind stress variability. von Schuckmann et al. (2008) showed that forcing an ocean model with daily wind stress forcing noticeably increased TIW activity compared to climatological wind forcing. Athié et al. (2009) confirmed the sensitivity of TIW activity to the choice of wind forcing, but noticed that overly energetic wind forcing might rather decrease TIW amplitudes. The observed increase in high-frequency wind stress variability could potentially ignite stronger TIWs through the eddy term of the barotropic energy conversion, but this hypothesis requires further attention in future research.

The expected consequences of the reported TIW intensification depend on the magnitudes of the changes in the SST budget terms, which influence, for instance, biomass production and large-scale wind patterns. The TIW-driven effects on the SST budget are, however, complex (Jochum & Murtugudde, 2006; Menkes et al., 2006). Aside from the observed increase in horizontal ETA (Figure 4), intensified TIWs are expected to cause stronger subsurface mixing and intensified sea surface cooling (Moum et al., 2009). However, the net effect of TIWs on the SST budget, and specifically the interplay of advection and vertical mixing due to TIWs, is still an open question (Moum et al., 2022).

This study serves as a first report on the observed long-term intensification of TIWs in the tropical North Atlantic. In particular, the net effect of intensified TIWs on the regional heat budget, and the distribution and variability of biogeochemical variables, require further studies with forced ocean models and coupled climate models. Whether the observed trends are externally forced by global warming or internally driven must also be addressed by model experiments and analysis of output from high-resolution (HighResMIP; Haarsma et al., 2016) models. It will be crucial to maintain in situ observing systems and to expand existing satellite missions in order to monitor and diagnose future changes of tropical Atlantic variability and to provide longer time series to disentangle warming-induced trends from interannual to multidecadal variability.

Data Availability Statement

Satellite observations used in this study are freely available at the following links: NOAA OI-SST version 2.1 (https://psl.noaa.gov/data/gridded/data.noaa.oisst.v2.highres.html), ESA-SSS-CCI version 3.21 (https://data.ceda.ac.uk/neodc/esacci/sea_surface_salinity/data/v03.21/7days), CMEMS-C3S-SLA version DT2021 (https://cds.climate.copernicus.eu/cdsapp#!/dataset/satellite-sea-level-global?tab=form). ECMWF ERA5 hourly 10-m horizontal wind speed is provided by the Copernicus Climate Data Store (https://cds.climate.copernicus.eu/cdsapp#!/dataset/reanalysis-era5-single-levels?tab=form). ERA-interim daily 10-m horizontal wind speed is provided by ECMWF (https://www.ecmwf.int/en/forecasts/datasets/reanalysis-datasets/era-interim). The near-surface drifter-wind-altimetry synthesis can be accessed via: ftp://ftp.aoml.noaa.gov/phod/pub/lumpkin/decomp/. Moored velocity observations at 0°, 23°W are provided through the World Data Center PANGAEA (https://doi.pangaea.de/10.1594/PANGAEA.941042). Current velocity data obtained by moored surface buoys at 4°N, 23°W and at 0°, 23°W are made available through the PIRATA program (https://www.pmel.noaa.gov/tao/drupal/disdel/). Surface velocities from the Ocean Surface Current Analyses Real-time (OSCAR) project are provided via the Physical Oceanography Distributed Active Archive Center (PODAAC): https://podaac-tools.jpl.nasa.gov/drive/files/allData/oscar/preview/L4/oscar_third_deg. MATLAB codes used to produce the results are available through zenodo: https://doi.org/10.5281/zenodo.7244863.

Acknowledgments
This research was performed while F.P.T. held a National Research Council (NRC) Research Associateship Award at NOAA's Atlantic Oceanographic and Meteorological Laboratory (AOML). R.C.P., G.R.F., and R.L. were supported by NOAA's Global Ocean Monitoring and Observing Program (funding reference number 100007298), under the PIRATA Northeast Extension project and Global Drifter Program, and by AOML. P.B. acknowledges support by the TRIATLAS project, which has received funding from the European Union's Horizon 2020 research and innovation programme under Grant agreement 817578. We thank Matthieu Le Hénaff and two reviewers for insightful comments on the manuscript. We also thank the captains, crews, scientists and technical groups involved in numerous research cruises to the tropical Atlantic that contributed to collecting shipboard and moored velocity data and making them freely available. Moored velocity observations were acquired by GEOMAR in cooperation with the PIRATA program supported by NOAA (USA), IRD and Meteo-France (France), INPE and the Brazil Navy (Brazil).

References

Ardhuin, F., Brandt, P., Gaultier, L., Donlon, C., Battaglia, A., Boy, F., et al. (2019). SKIM, a candidate satellite mission exploring global ocean currents and waves. *Frontiers in Marine Science*, *6*, 209. https://doi.org/10.3389/fmars.2019.00209

Ascani, F., Firing, E., Dutrieux, P., McCreary, J. P., & Ishida, A. (2010). Deep equatorial ocean circulation induced by a forced-dissipated Yanai beam. *Journal of Physical Oceanography*, *40*(5), 1118–1142. https://doi.org/10.1175/2010JPO4356.1

Ascani, F., Firing, E., McCreary, J. P., Brandt, P., & Greatbatch, R. J. (2015). The deep equatorial ocean circulation in wind-forced numerical solutions. *Journal of Physical Oceanography*, *45*(6), 1709–1734. https://doi.org/10.1175/JPO-D-14-0171.1

Athié, G., & Marin, F. (2008). Cross-equatorial structure and temporal modulation of intraseasonal variability at the surface of the Tropical Atlantic Ocean. *Journal of Geophysical Research*, *113*(C8), C08020. https://doi.org/10.1029/2007JC004332

Athié, G., Marin, F., Treguier, A.-M., Bourlès, B., & Guiavarc'h, C. (2009). Sensitivity of near-surface Tropical Instability Waves to submonthly wind forcing in the tropical Atlantic. *Ocean Modelling*, *30*(4), 241–255. https://doi.org/10.1016/j.ocemod.2009.06.016

Bastin, S., Claus, M., Brandt, P., & Greatbatch, R. J. (2020). Equatorial deep jets and their influence on the mean equatorial circulation in an idealized ocean model forced by intraseasonal momentum flux convergence. *Geophysical Research Letters*, *47*(10), e2020GL087808. https://doi.org/10.1029/2020GL087808

Bourlès, B., Araujo, M., McPhaden, M. J., Brandt, P., Foltz, G. R., Lumpkin, R., et al. (2019). PIRATA: A sustained observing system for tropical Atlantic climate research and forecasting. *Earth and Space Science*, *6*(4), 577–616. https://doi.org/10.1029/2018EA000428

Boutin, J., Vergely, J.-L., Reul, N., Catany, R., Koehler, J., Martin, A., & Coauthors (2021). ESA sea surface salinity climate change initiative (Sea_Surface_Salinity_cci): Weekly and monthly sea surface salinity products, v03.21, for 2010 to 2020. *NERC EDS Centre for Environmental Data Analysis*. https://doi.org/10.5285/5920a2c77e3c45339477acd31ce62c3c

Brandt, P., Hahn, J., Schmidtko, S., Tuchen, F. P., Kopte, R., Kiko, R., et al. (2021). Atlantic equatorial undercurrent intensification counteracts warming-induced deoxygenation. *Nature Geoscience*, *14*(5), 278–282. https://doi.org/10.1038/s41561-021-00716-1

Brandt, P., Schott, F. A., Provost, C., Kartavtseff, A., Hormann, V., Bourlès, B., & Fischer, J. (2006). Circulation in the central equatorial Atlantic: Mean and intraseasonal to seasonal variability. *Geophysical Research Letters*, *33*(7), L07609. https://doi.org/10.1029/2005GL025498

Bunge, L., Provost, C., & Kartavtseff, A. (2007). Variability in horizontal current velocities in the central and eastern equatorial Atlantic in 2002. *Journal of Geophysical Research*, *112*(C2), C02014. https://doi.org/10.1029/2006JC003704

Caltabiano, A. C. V., Robinson, I. S., & Pezzi, L. P. (2005). Multi-year satellite observations of instability waves in the Tropical Atlantic Ocean. *Ocean Science*, *1*(2), 97–112. https://doi.org/10.5194/os-1-97-2005

de Decco, H. T., Torres Junior, A. R., Pezzi, L. P., & Landau, L. (2018). Revisiting tropical instability wave variability in the Atlantic ocean using SODA reanalysis. *Ocean Dynamics*, *68*(3), 327–345. https://doi.org/10.1007/s10236-017-1128-2

Eddebbar, Y. A., Subramanian, A. C., Whitt, D. B., Long, M. C., Verdy, A., Mazloff, M. R., & Merrifield, M. A. (2021). Seasonal modulation of dissolved oxygen in the equatorial Pacific by tropical instability vortices. *Journal of Geophysical Research: Oceans*, *126*(11), e2021JC017567. https://doi.org/10.1029/2021JC017567

Foltz, G. R., Brandt, P., Richter, I., Rodríguez-Fonseca, B., Hernandez, F., Dengler, M., et al. (2019). The tropical Atlantic observing system. *Frontiers in Marine Science*, *6*, 206. https://doi.org/10.3389/fmars.2019.00206

Foltz, G. R., Carton, J. A., & Chassignet, E. P. (2004). Tropical instability vortices in the Atlantic Ocean. *Journal of Geophysical Research*, *109*(C3), C03029. https://doi.org/10.1029/2003JC001942

Foltz, G. R., Grodsky, S. A., Carton, J. A., & McPhaden, M. J. (2003). Seasonal mixed layer heat budget of the tropical Atlantic Ocean. *Journal of Geophysical Research*, *108*(C5), 3146. https://doi.org/10.1029/2002JC001584

Foltz, G. R., Hummels, R., Dengler, M., Perez, R. C., & Araujo, M. (2020). Vertical turbulent cooling of the mixed layer in the Atlantic ITCZ and trade wind regions. *Journal of Geophysical Research: Oceans*, *125*(2), e2019JC015529. https://doi.org/10.1029/2019JC015529

Greatbatch, R. J., Claus, M., Brandt, P., Matthießen, J.-D., Tuchen, F. P., Ascani, F., et al. (2018). Evidence for the maintenance of slowly varying equatorial currents by intraseasonal variability. *Geophysical Research Letters*, *45*(4), 1923–1929. https://doi.org/10.1002/2017GL076662

Grodsky, S. A., Carton, J. A., & McClain, C. R. (2008). Variability of upwelling and chlorophyll in the equatorial Atlantic. *Geophysical Research Letters*, *35*(3), L03610. https://doi.org/10.1029/2007GL032466

Grodsky, S. A., Carton, J. A., Provost, C., Servain, J., Lorenzzetti, J. A., & McPhaden, M. J. (2005). Tropical instability waves at 0°N, 23°W in the Atlantic: A case study using pilot research moored array in the tropical Atlantic (PIRATA) mooring data. *Journal of Geophysical Research*, *110*(C8), C08010. https://doi.org/10.1029/2005JC002941

Haarsma, R. J., Roberts, M. J., Vidale, P. L., Senior, C. A., Bellucci, A., Bao, Q., et al. (2016). High resolution model intercomparison project (HighResMIP v1.0) for CMIP6. *Geoscientific Model Development*, *9*(11), 4185–4208. https://doi.org/10.5194/gmd-9-4185-2016

Heukamp, F. O., Brandt, P., Dengler, M., Tuchen, F. P., McPhaden, M. J., & Moum, J. N. (2022). Tropical instability waves and wind-forced cross-equatorial flow in the central Atlantic Ocean. *Geophysical Research Letters*, *49*(19), e2022GL099325. https://doi.org/10.1029/2022GL099325

Hu, S., Sprintall, J., Guan, C., McPhaden, M. J., Wang, F., Hu, D., & Cai, W. (2020). Deep-reaching acceleration of global mean ocean circulation over the past two decades. *Science Advances*, *6*, eaax7727. https://doi.org/10.1126/sciadv.aax7727

Huang, B., Liu, C., Banzon, V., Freeman, E., Graham, G., Hankins, B., et al. (2021). Improvements of the daily optimum interpolation sea surface temperature (DOISST) version 2.1. *Journal of Climate*, *34*(8), 2923–2939. https://doi.org/10.1175/JCLI-D-20-0166.1

Hummels, R., Dengler, M., & Bourlès, B. (2013). Seasonal and regional variability of upper ocean diapycnal heat flux in the Atlantic cold tongue. *Progress in Oceanography*, *111*, 52–74. https://doi.org/10.1016/j.pocean.2012.11.001

Hummels, R., Dengler, M., Brandt, P., & Schlundt, M. (2014). Diapycnal heat flux and mixed layer heat budget within the Atlantic Cold Tongue. *Climate Dynamics*, *43*(11), 3179–3199. https://doi.org/10.1007/s00382-014-2339-6

Inoue, R., Lien, R.-C., Moum, J. N., Perez, R. C., & Gregg, M. C. (2019). Variations of equatorial shear, stratification, and turbulence within a tropical instability wave cycle. *Journal of Geophysical Research: Oceans*, *124*(3), 1858–1875. https://doi.org/10.1029/2018JC014480

Jochum, M., Cronin, M. F., Kessler, W. S., & Shea, D. (2007). Observed horizontal temperature advection by tropical instability waves. *Geophysical Research Letters*, *34*(9), L09604. https://doi.org/10.1029/2007GL029416

Jochum, M., Malanotte-Rizzoli, P., & Busalacchi, A. (2004). Tropical instability waves in the Atlantic Ocean. *Ocean Modelling*, *7*(1–2), 145–163. https://doi.org/10.1016/S1463-5003(03)00042-8

Jochum, M., & Murtugudde, R. (2004). Internal variability of the tropical Pacific ocean. *Geophysical Research Letters*, *31*(14), L14309. https://doi.org/10.1029/2004GL020488

Jochum, M., & Murtugudde, R. (2006). Temperature advection by tropical instability waves. *Journal of Physical Oceanography*, *36*(4), 592–605. https://doi.org/10.1175/JPO2870.1

Kennan, S. C., & Flament, P. J. (2000). Observations of a tropical instability vortex. *Journal of Physical Oceanography*, *30*(9), 2277–2301. https://doi.org/10.1175/1520-0485(2000)030<2277:OOATIV>2.0.CO;2

Körner, M., Claus, M., Brandt, P., & Tuchen, F. P. (2022). Sources and pathways of intraseasonal meridional kinetic energy in the equatorial Atlantic Ocean. *Journal of Physical Oceanography*, *52*(10), 2445–2462. https://doi.org/10.1175/JPO-D-21-0315.1

Lee, T., Lagerloef, G., Kao, H.-Y., McPhaden, M. J., Willis, J., & Gierach, M. M. (2014). The influence of salinity on tropical Atlantic instability waves. *Journal of Geophysical Research: Oceans*, *119*(12), 8375–8493. https://doi.org/10.1002/2014JC010100

Lumpkin, R., & Garzoli, S. L. (2005). Near-surface circulation in the Tropical Atlantic Ocean. *Deep Sea Research Part I*, *52*(3), 495–518. https://doi.org/10.1016/j.dsr.2004.09.001

Lumpkin, R., & Garzoli, S. L. (2011). Interannual to decadal changes in the Western South Atlantic's surface circulation. *Journal of Geophysical Research*, *116*(C1), C01014. https://doi.org/10.1029/2010JC006285

Masina, S., Philander, S. G. H., & Bush, A. B. G. (1999). An analysis of tropical instability waves in a numerical model of the Pacific ocean: 2. Generation and energetics of the waves. *Journal of Geophysical Research*, *104*(C12), 29637–29661. https://doi.org/10.1029/1999JC900226

Menkes, C. E. R., Kennan, S. C., Flament, P. J., Dandonneau, Y., Masson, S., Biessy, B., & Coauthors (2002). A whirling ecosystem in the equatorial Atlantic. *Geophysical Research Letters*, *29*(11), 1553. https://doi.org/10.1029/2001GL014576

Menkes, C. E. R., Vialard, J. G., Kennan, S. C., Boulanger, J.-P., & Madec, G. V. (2006). A modeling study of the impact of tropical instability waves on the heat budget of the eastern equatorial Pacific. *Journal of Physical Oceanography*, *36*(5), 847–865. https://doi.org/10.1175/JPO2904.1

Moum, J. N., Hughes, K. G., Shroyer, E. L., Smyth, W. D., Cherian, D., Warner, S. J., et al. (2022). Deep cycle turbulence in Atlantic and Pacific cold tongues. *Geophysical Research Letters*, *49*(8), e2021GL097345. https://doi.org/10.1029/2021GL097345

Moum, J. N., Lien, R.-C., Perlin, A., Nash, J. D., Gregg, M. C., & Wiles, P. J. (2009). Sea surface cooling at the equator by subsurface mixing in tropical instability waves. *Nature Geoscience*, *2*(11), 761–765. https://doi.org/10.1038/NGEO657

Olivier, L., Reverdin, G., Hasson, A., & Boutin, J. (2020). Tropical instability waves in the Atlantic Ocean: Investigating the relative role of sea surface salinity and temperature from 2010 to 2018. *Journal of Geophysical Research: Oceans*, *125*(12), e2020JC016641. https://doi.org/10.1029/2020JC016641

Peng, Q., Xie, S.-P., Wang, D., Huang, R. X., Chen, G., Shu, Y., et al. (2022). Surface warming-induced global acceleration of upper ocean currents. *Science Advances*, *8*(16), eabj8394. https://doi.org/10.1126/sciadv.abj8394

Perez, R. C., Foltz, G. R., Lumpkin, R., & Schmid, C. (2019). Direct measurements of upper ocean horizontal velocity and vertical shear in the tropical North Atlantic at 4°N, 23°W. *Journal of Geophysical Research: Oceans*, *124*(6), 4133–4151. https://doi.org/10.1029/2019JC015064

Perez, R. C., Lumpkin, R., Johns, W. E., Foltz, G. R., & Hormann, V. (2012). Interannual variations of Atlantic tropical instability waves. *Journal of Geophysical Research*, *117*(C3), C03011. https://doi.org/10.1029/2011JC007584

Peter, A.-C., Le Hénaff, M., du Penhoat, Y., Menkes, C. E. R., Marin, F., Vialard, J. G., et al. (2006). A model study of the seasonal mixed layer heat budget in the equatorial Atlantic. *Journal of Geophysical Research*, *111*(C6), C06014. https://doi.org/10.1029/2005JC003157

Radenac, M.-H., Jouanno, J., Tchamabi, C. C., Awo, M., Bourlès, B., Arnault, S., & Aumont, O. (2020). Physical drivers of the nitrate seasonal variability in the Atlantic cold tongue. *Ocean Science*, *17*(2), 529–545. https://doi.org/10.5194/bg-17-529-2020

Rodríguez, E., Bourassa, M., Chelton, D., Farrar, J. T., Long, D., Perkovic-Martin, D., & Samelson, R. (2019). The winds and currents mission concept. *Frontiers in Marine Science*, *6*, 438. https://doi.org/10.3389/fmars.2019.00438

Seo, H., Jochum, M., Murtugudde, R., Miller, A. J., & Roads, J. O. (2007). Feedback of tropical instability-wave-induced atmospheric variability onto the Ocean. *Journal of Climate*, *20*(23), 5842–5855. https://doi.org/10.1175/JCLI4330.1

Seo, H., & Xie, S.-P. (2011). Response and impact of equatorial ocean dynamics and tropical instability waves in the tropical Atlantic under global warming: A regional coupled downscaling study. *Journal of Geophysical Research*, *116*(C3), C03026. https://doi.org/10.1029/2010JC006670

Sherman, J., Subramaniam, A., Gorbunov, M. Y., Fernández-Carrera, A., Kiko, R., Brandt, P., & Falkowski, P. G. (2022). The photophysiological response of nitrogen-limited phytoplankton to episodic nitrogen supply associated with tropical instability waves in the equatorial Atlantic. *Frontiers in Marine Science*, *8*, 814663. https://doi.org/10.3389/fmars.2021.814663

Shi, W., & Wang, M. (2021). Tropical instability wave modulation of chlorophyll-a in the equatorial Pacific. *Scientific Reports*, *11*(1), 22517. https://doi.org/10.1038/s41598-021-01880-5

Specht, M. S., Jungclaus, J., & Bader, J. (2021). Identifying and characterizing subsurface tropical instability waves in the Atlantic Ocean in simulations and observations. *Journal of Geophysical Research: Oceans*, *126*(10), e2020JC017013. https://doi.org/10.1029/2020JC017013

Tuchen, F. P., Brandt, P., Claus, M., & Hummels, R. (2018). Deep intraseasonal variability in the central equatorial Atlantic. *Journal of Physical Oceanography*, *48*(12), 2851–2865. https://doi.org/10.1175/JPO-D-18-0059.1

Tuchen, F. P., Brandt, P., Hahn, J., Hummels, R., Krahmann, G., Bourlès, B., et al. (2022). Two decades of full-depth current velocity observations from a moored observatory in the central equatorial Atlantic at 0°N, 23°W. *Frontiers in Marine Science*, *9*, 910979. https://doi.org/10.3389/fmars.2022.910979

Tuchen, F. P., Brandt, P., Lübbecke, J. F., & Hummels, R. (2022). Transports and pathways of the tropical AMOC return flow from argo data and shipboard velocity measurements. *Journal of Geophysical Research: Oceans*, *127*(2), e2021JC018115. https://doi.org/10.1029/2021JC018115

Tuchen, F. P., Lübbecke, J. F., Brandt, P., & Fu, Y. (2020). Observed transport variability of the Atlantic subtropical cells and their connection to tropical sea surface temperature variability. *Journal of Geophysical Research: Oceans*, *125*(12), e2020JC016592. https://doi.org/10.1029/2020JC016592

von Schuckmann, K., Brandt, P., & Eden, C. (2008). Generation of tropical instability waves in the Atlantic Ocean. *Journal of Geophysical Research*, *113*(C8), C08034. https://doi.org/10.1029/2007JC004712

Weisberg, R. H., & Weingartner, T. J. (1988). Instability waves in the equatorial Atlantic Ocean. *Journal of Physical Oceanography*, *18*(11), 1641–1657. https://doi.org/10.1175/1520-0485(1988)018<1641:IWITEA>2.0.CO;2

Wenegrat, J. O., & McPhaden, M. J. (2015). Dynamics of the surface layer diurnal cycle in the equatorial Atlantic Ocean (0°, 23°W). *Journal of Geophysical Research: Oceans*, *120*(1), 563–581. https://doi.org/10.1002/2014JC010504

Wu, Q., & Bowman, K. P. (2007a). Interannual variations of tropical instability waves observed by the Tropical Rainfall Measuring Mission. *Geophysical Research Letters*, *34*(9), L09701. https://doi.org/10.1029/2007GL029719

Wu, Q., & Bowman, K. P. (2007b). Multiyear satellite observations of the atmospheric response to Atlantic tropical instability waves. *Journal of Geophysical Research*, *112*(D19), D19104. https://doi.org/10.1029/2007JD008627

Wunsch, C. (2020). Is the Ocean speeding up? Ocean Surface energy trends. *Journal of Physical Oceanography*, *50*(11), 3205–3217. https://doi.org/10.1175/JPO-D-20-0082.1

Yu, Z., McCreary, J. P., Jr., & Proehl, J. A. (1995). Meridional asymmetry and energetics of tropical instability waves. *Journal of Physical Oceanography*, *25*(12), 2997–3007. https://doi.org/10.1175/1520-0485(1995)025<2997:MAAEOT>2.0.CO;2

References From the Supporting Information

Hersbach, H., Bell, B., Berrisford, P., Hirahara, S., Horányi, A., Muñoz-Sabater, J., et al. (2020). The ERA5 global reanalysis. *Quarterly Journal of the Royal Meteorological Society*, *146*(730), 1999–2049. https://doi.org/10.1002/qj.3803

Lagerloef, G. S. E., Mitchum, G. T., Lukas, R. B., & Niiler, P. P. (1999). Tropical Pacific near-surface currents estimated from altimeter, wind, and drifter data. *Journal of Geophysical Research*, *104*(C10), 23313–23326. https://doi.org/10.1029/1999JC900197